SCIENTIFIC REPORTS

OPEN

Role of the Interplay Between the Internal and External Conditions in Invasive Behavior of Tumors

Received: 28 June 2017
Accepted: 4 April 2018
Published online: 13 April 2018

Youness Azimzade[1], Abbas Ali Saberi[1,2] & Muhammad Sahimi[3]

Tumor growth, which plays a central role in cancer evolution, depends on both the internal features of the cells, such as their ability for unlimited duplication, and the external conditions, e.g., supply of nutrients, as well as the dynamic interactions between the two. A stem cell theory of cancer has recently been developed that suggests the existence of a subpopulation of self-renewing tumor cells to be responsible for tumorigenesis, and is able to initiate metastatic spreading. The question of abundance of the cancer stem cells (CSCs) and its relation to tumor malignancy has, however, remained an unsolved problem and has been a subject of recent debates. In this paper we propose a novel model beyond the standard stochastic models of tumor development, in order to explore the effect of the density of the CSCs and oxygen on the tumor's invasive behavior. The model identifies natural selection as the underlying process for complex morphology of tumors, which has been observed experimentally, and indicates that their invasive behavior depends on both the number of the CSCs and the oxygen density in the microenvironment. The interplay between the external and internal conditions may pave the way for a new cancer therapy.

Cancer usually begins with out-of-order duplication of a single cell that has stem cell-like behavior, referred to as the cancer stem cell (CSC)[1]. Based on the CSC hypothesis, a CSC can duplicate without limit and differentiate[2]. The classical CSC hypothesis proposes that, among all cancerous cells, only "a few" act as stem cells, but studies have reported[3] that a relatively high proportion of the cells are tumorigenic, contradicting the general belief. The CSCs have been proposed as the driving force for tumorigenesis and the seeds for metastases[4]. Their decisive role in maintaining capacity for malignant proliferation, invasion, metastasis, and tumor recurrence has been reported frequently[5]. For example, CSCs of breast tumor are involved in spontaneous metastases in mouse models[6]. Moreover, CSCs promote the metastatic and invasive ability of melanoma[7] and their prsence is correlated with invasive behavior at colorectal adenocarcinoma[8]. The effect of the number of CSCs on tumor morphology has been the subject of several experimental studies and simulation. Based on simulations[9,10], the frequency of the CSCs smoothens the morphology of tumor, and based on an experimental study[11], the number of CSCs is higher in tumors with medium invasiveness (the so-called Gleason grade) than tumors with lower (Gleason grade) and higher (Gleason grade) invasiveness. The relation between tumor malignancy and the frequency of the CSCs needs, however, more clarification[4].

Cancerous cells use oxygen to produce metabolites for duplication and growth[12]. Experimental *in-vivo*[13] and *in-vitro*[14] studies, as well as computer simulations[15,16], have reported that the density of oxygen regulates tumor morphology and its shortage drives morphological irregularities. Due to the apparent strong correlations between the tumors' shape and their malignancy, fractal characterization of tumors has been used as a diagnostic assay for various types of tumors[17–19]. However, there is still no explanation as to why cellular structures at the scale of tumors display self-similar characteristics[20]. of well-known physical phenomena, including diffusion and reaction-diffusion, as well as percolation, surface growth, and models of phase transition[21].

In this paper we propose a novel model to study the effect of the number of the CSCs and the oxygen's density on the invasive behavior of a general type of cancer. As we show below, the development of irregular shapes and the respective tumor's invasive behavior are correlated with the two factors. Unlike the previous studies, we present a quantitative measure by which one can understand better the effect of completion on the malignancy of

[1]Department of Physics, University of Tehran, Tehran, 14395-547, Iran. [2]Institut für Theoretische Physik, Universitat zu Köln, Zülpicher Strasse 77, Köln, 50937, Germany. [3]Mork Family Department of Chemical Engineering Materials Science, University of Southern California, Los Angeles, California, 90089-1211, USA. Correspondence and requests for materials should be addressed to A.A.S. (email: ab.saberi@ut.ac.ir)

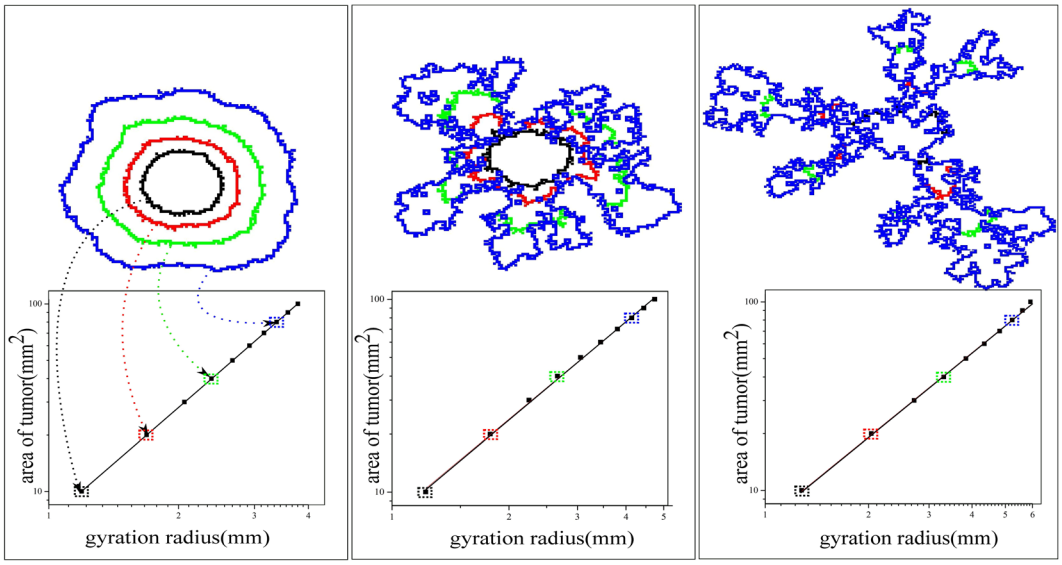

Figure 1. Fractal structure of the tumors. Tumors are irregular, but exhibit self-similarity. The linearity of the plot indicates fractal behavior, with the slope being $D_f \approx 1.99 \pm 0.01$ for $p_s = 0.1$ (left), 1.76 ± 0.02 for $p_s = 0.5$ (middle), and 1.47 ± 0.02 for $p_s = 1$ (right), with (normalized) oxygen density, $n = 1$. Each contour line represents the borderline of the tumor with the corresponding gyration radius indicated by the dotted arrows. It should be noted that the figure on the left covers 5000 units (50 mm^2) in 5000 time steps (30 days), while the ones in the middle and right cover the same area in 14000 (55 days) and 12000 (83 days) steps, respectively. The simulations were carried out in a 200×200 lattice

tumors. We take the shape irregularity as the factor for identifying the invasive behavior of tumor and compare our results with experimental reports. The model that we present contains the essential features of the cells, such as symmetric/asymmetric division, metabolic state, cellular quiescence and movements, apoptosis, and existence of oxygen and its consumption. Our results explain, for the first time to our knowledge, the aforementioned experimentally-observed fractal behavior and contradict the predictions of recent models for the relation between the number of the CSCs and the growth rate and invasion. In addition, we believe that the results may cast doubt on the recent therapeutic approach based on oxygen deprivation.

Results

As the system evolves, the cells consume oxygen, enhance their metabolic state, and proliferate after reaching the energy level of u_p, in order to create a clone - the tumor - see Fig. 1. The perimeter of the clone is the main object that we study in this paper.

As Fig. 1 demonstrates, the cells take on irregular shapes during their growth whose complexity depends on the number of the CSCs (or probability p_s). One interesting approach is to study the structure of the perimeters in the context of interface instability[22–24]. The analogy with the instability of interfaces has been established for the case of melanoma[25], and the instabilities were attributed to nutrient density. But, here, we quantify tumor behavior through classifying irregular morphology of the tumors. To quantify the irregularity of the tumor's morphology and its evolution, we use fractal analysis. To this end, we measure the average distance r from the center of the mass, as well as the area of the tumor during its growth. Figure 1 indicates that log(area) versus log r is a linear plot so that, area $\sim r^{D_f}$. Thus, the slope of the line in the logarithmic plot is the fractal dimension D_f, implying self-similarity of the tumors of various sizes. The self-similarity of the tumors' growth is the result of heterogeneous duplication on their perimeter, which itself is due to the oxygen gradient. Cells in the region with higher curvatures have better supply of oxygen, helping them increase their metabolic state, and proliferate faster. The proliferation also creates new perimeter curvature with the same behavior. As the number of oxygen consumers, which is proportional to p_s, increases the competition between the cells for the limited oxygen supply intensifies and oxygen availability becomes more heterogeneous. Thus, the tumors take on more irregular shapes or lower fractal dimension D_f, contradicting previous studies[9,10] that proposed an adverse relation between the number of the CSCs and the invasive behavior.

We note that fractal scaling has been reported previously in the experimental studies[17,18]. Moreover, irregular shapes have been interpreted as an indication of invasive behavior of various tumors[17–19]. Tumors with more irregular shapes are more invasive, and in our model the more irregular tumors have smaller D_f. There are several reports that confirm the correlation between D_f and tumor malignancy (a malignant tumor possesses a lower fractal dimension than that of a benign mass)[26–29].

A study of the variations of D_f with p_s and the density n of the oxygen is useful to characterization of the tumor behavior. The computed D_f for various values of p_s and oxygen densities is shown in Fig. 2.

Figure 2 presents explicitly the value of D_f and the corresponding malignancy of tumor as a result of both the internal feature and the external conditions. For a fixed density n of oxygen, the invasive behavior of tumor always

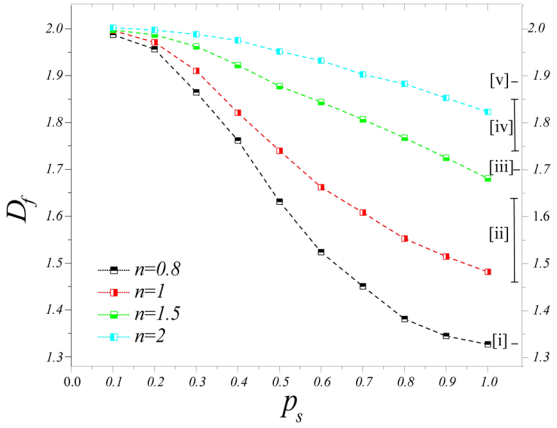

Figure 2. Interrelationship between malignancy, immortality and oxygen density. Fractal dimension D_f as an indication of malignancy for various tumors. Our model reproduces some of the previously reported fractal dimensions: [i] $D_f \sim 1.338 \pm 0.248$[30]; [ii] $1.46 \lesssim D_f \lesssim 1.64$[29]; [iii] $D_f \sim 1.696 \pm 0.009$; [iv] $1.74 \lesssim D_f \lesssim 1.85$[31], and [v] $D_f \sim 1.887 \pm 0.008$[32].

increases with p_s, implying that, regardless of the environmental conditions, higher numbers of CSCs always lead to a more invasive behavior; see Fig. 2 in the Supplementary Information (SI). This is in contradiction with the existing reports on the adverse effect of p_s on the tumor's invasive behavior[9,10]. On the other hand, the effect of the environmental stress on invasion is regulated by internal feature of the cells, p_s. For $p_s = 1$, the oxygen deprivation significantly increases the malignant behavior of tumors, while for $p_s = 0$, the density of oxygen has negligible effect on tumor's invasive behavior.

Relation to Superficial Spreading Melanoma

As presented here, our model explains a two-dimensional (2D) tumor growth. Early stages of Superficial Spreading melanoma has a 2D structure that might be a promising case to apply our findings to. Experiments indicate that there is no blood flow to the Superficial Spreading melanoma (SSM) with thickness less than 0.9 mm[33]. In addition, melanoma is, at least in its early stages, an approximately 2D phenomenon, so that a 2D model may properly produce its structure. The malignant cells in SSM stay within the original tissue - the epidermis - in an *in-situ* phase for a long time, which could be up to decades. Initially, the SSM grows horizontally on the skin surface, known as *radial growth*, with lesion indicated by a slowly-enlarging flat area of discolored skin. Then, part of the SSM becomes invasive, crossing the base membrane and entering the dermis, giving rise to a rapidly-growing nodular melanoma within the SSM that begins to proliferate more deeply within skin.

Discussion

The proposed model sheds new light on and provides new insight into the invasive behavior of tumors by deciphering the effect of both intrinsic and extrinsic features of cells. It also demonstrates that elimination of the oxygen in the previous models gives rise to such a relation. The fractal behavior that we identify and attribute to the growth limited to the perimeter is similar to surface growth[17,34]. Nevertheless, close inspection of the proliferation activity in the perimeter in the proposed model reveals larger parts of the cells as proliferative cells; see Fig. 1 of the SI. As the model demonstrates, a single biological parameter, namely p_s, changes the cell's features and results collectively in various self-similar states with distinct fractal dimensions. Previous models, which considered the CSCs[9,10], obtained an inverse relation between the number of the CSCs and invasion, but our model indicates increased malignancy to be proportional to larger numbers of the CSCs. Compared to experimental data[11] our model confirms increasing of morphological irregularities (Gleason grade), but complete consistency require more biological details in the model.

Tumors with low number of the CSCs that were proposed by the previous studies[9,35] did not respond to oxygen deprivation, as was expected[13,14]. Hence, tumors that respond to oxygen deprivation must have larger number of the CSCs. In addition, models that do not consider the CSC evolution and endow the cells with unlimited proliferation capacity[14,15] produce tumors corresponding to $p_s = 1$. Such models consider the effect of oxygen and, as our model confirms, oxygen deprivation leads to higher irregularities. As p_s decreases, the effect of oxygen vanishes. Thus, a lower number of the CSCs, which was proposed previously[9,35], does not conform to the experimentally well-established oxygen effects. Our model, in addition to reproducing such result, provides quantitative and comparable results to classify the irregularities that can be used to analyze experimental data that have been reported for the fractal dimensions.

The conceptual results are applicable to the growth of other solid tumors that display the aforementioned behavior in response to oxygen tension and frequency of CSCs. For example, in the case of the SSM in which the number of CSCs is not small[3,36], oxygen deprivation probably increases tumor malignancy. Contrary to the previous studies, the present model predicts invasion as the result of *both* the tumor *and* the microenvironment, demonstrating the effect of nutrient deprivation on the invasion. This implies that recent studies on such therapeutic approach[37,38] must consider carefully the side effects that, based on our model for tumors with larger numbers of the CSCs, can increase tumor malignancy.

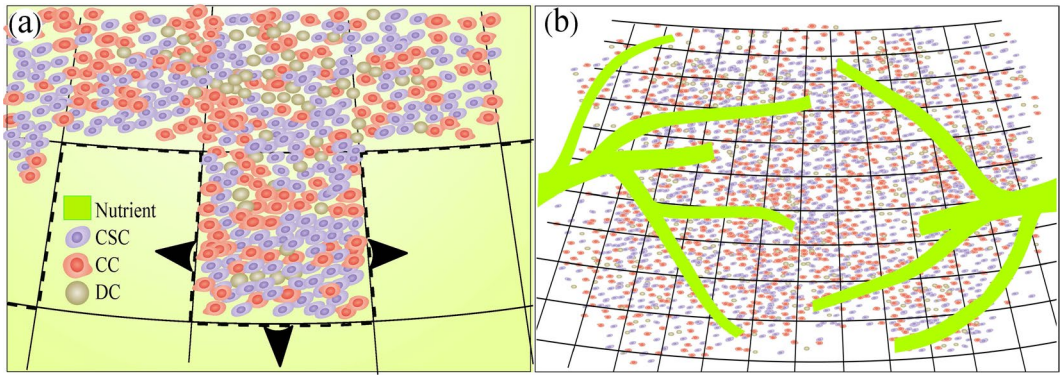

Figure 3. Schematic of the model. (**a**) Various types of cells that are either proliferating or dying. Nutrient density in the milieu is constant and after diffusing from the surrounding is consumed by the cells. (**b**) An alternative mechanism for oxygen supply by the capillaries coming from the third dimension to feed the tumor at random sites. The results do not depend on the choice of the initial/boundary conditions for the nutrient; see the SI.

The Model

Similar to many other natural systems, biological media fluctuate due to the intrinsic randomness of the individual events[39]. Cells are involved in regulatory pathways that depend highly nonlinearly on the chemical species that are present in low copy numbers per cell[40], as a result of which other factors, such as the forces between cells, fluctuate significantly[41]. Thus, statistical approaches are suitable for simulating cells' behavior. We consider the 2D lattice shown in Fig. 3 in which each bond is 100 micrometer long, while each site has the capacity for 100 cancer cells that typically have 10 μm diameter[42]. The nutrient density is constant on the perimeter of a circle with a radius of 1 cm. It diffuses into the internal zones and is consumed by the living cells. In the SI we present the results for various other initial/boundary conditions for the oxygen supply, including smaller and larger radii of the circle, regular and random distribution of the oxygen source, as well as its uniform distribution in the medium, and show that the predictions of the model do not depend on the choice of the oxygen supply mechanism. Though we consider 2D structures, the results for a 3D structure for oxygen supply system (vessels and capillaries) would remain qualitatively the same, while the model can be extended to 3D.

Keeping the oxygen density uniform in the milieu -0.15 mol/ml[16] - a CSC is inserted at the center of the medium that consumes the oxygen and enhances its metabolic state. Although metabolic pathways are not fully understood, metabolic activity is a crucial factor in a cell's decision to either proliferate or die[43]. In the former case a cell must increase its biomass and replicate its genome prior to division, in order to create two daughter cells. Thus, the cell must generate enough energy and acquire or synthesize biomolecules at a sufficient rate to meet the proliferation demand[44]. Given such biological facts, we choose metabolic state as the decisive factor for a cell's decision to proliferate, and define an internal energy u_{cell} for each cell as an indicator of its metabolic state. Physically, the cells acquire energy from the environment to accumulate internal energy[45] - the energy of the absorbed molecules - which evolves according to the energy conservation law:

$$\frac{\partial u_{\text{cell}}}{\partial t} = \chi n(x, y, t) - \gamma u_{\text{cell}}, \tag{1}$$

where $n(x, y, t)$ is the oxygen density at position (x, y) and time t, with χ and γ being positive constants related to energy accumulation and consumption rate (for details of all the constants and their values see Table 1 in the SI). If a cell's energy reaches a threshold u_p, it will begin duplication. We set u_p, χ and γ such that every cell in the appropriate situation will be in the duplication state after 15 hours[46], which is about the time that tumor cells need to reach the so-called cell checkpoints eG_1 (early G_1), G_1 and eS in the cell cycle for division. G_1 is the primary point at which a cell must decide whether to divide. After it passes G_1 and enters the S phase, the cell is committed to division[46] (other checkpoints, such as G_2 at which the cell is mostly concerned with the condition of its DNA, still remain to be completed in the next step). As we show below, Eq. (1) together with the limits imposed, reproduces cell plasticity and various proliferation activities under a variety of external conditions[47] that were reported recently[46]. Time is measured in units of 10 minutes.

The evolution of the internal energy u_{cell} of the cells depends on the local density of oxygen through a set of coupled differential equations, and if enough oxygen exists at the position of the first CSC, u_{cell} increases to u_p and the first CSC duplicates into two daughter cells. This relation between oxygen density, cell metabolic state and its duplication dynamics ensures the apparent role of the oxygen density in the tumor evolution. One may consider various scenarios for quantitative studies of the CSC proliferation[48–51], but the probability of distinct kinds of divisions has yet to be assessed experimentally. Besides, some other studies[52] have proposed the cells' self-renewal ability as the prerequisite for tumor maintenance. Thus, we choose the simplest biologically-correct model that has the ability to generate the entire possible range of the CSC population percentage, from zero up to the values produced by the various mathematical[48–51] and biological models[52]. In this model, during duplication of each CSC one daughter cell is assumed to be CSC, while the second one is either a CSC with probability p_s - the probability of symmetric duplication of the CSCs - or a cancerous cell (CC) with probability $(1 - p_s)$; see Fig. 4. Each CC duplicates into two CCs if it is allowed to[10]. Such a probabilistic approach is motivated by the fact stated

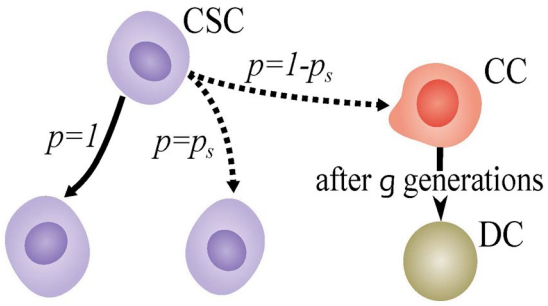

Figure 4. Division of the cells. During division each CSC creates another CSC. The other daughter cell would either be a CSC with probability p_s or a CC with probability $1 - p_s$. Each CC creates two CCs during duplication, if it is capable of division. The CSCs can continue the division process for a long time, whereas each CC loses its ability for duplicating after g divisions, and dies. Clearly, the first CC daughters could duplicate $g - 1$ times, where we set $g = 5$[10].

earlier, that according to the classical CSC hypothesis, among all cancerous cells, only "a few" act as stem cells, whereas some studies[3,53] have reported that the population of CSCs can be relatively high, which is why we take the population of the CSCs (with probability p_s) as a parameter of our model. For $p_s = 1$ the model reduces to the stochastic model of tumor development[54]. Every CSC continues such a division for an unlimited frequency, but the CC can have only limited generations of duplication[55], which we set it to be $g = 5$[1,10] after which it will die and produce dead cells (DCs); see Fig. 4. As the cells undergo apoptosis, they are recognized and removed from the body by phagocytes. Thus, we assume that the dead cells remain inactive in the medium, but even if we eliminate them after death, the main results remain the same; see the Fig. S15 in the SI.

We define the density of cells of type i at location (x, y) at time t by,

$$C_i(x, y, t) = \frac{\text{number of cells at } (x, y, t)}{\text{capacity of each site}}, \tag{2}$$

with $i \equiv$ CSCs, CCs, and DCs. Equation (2) is also valid for the total density of cells, $C_t = C_{CSC} + C_{CC} + C_{DC}$. Recall also that the capacity of each site is 100 cells[42]. The density of the CCs is denoted by $C_{CC}(x, y, t; j)$ in which j indicates their generation that varies from 1 to g (after g generations they produce the DCs). Healthy tissues contain healthy cells in which the distribution of the nutrients is in a steady state. We eliminate the healthy cells for all the tumors, as our results are based on comparison with and differences of tumors' behavior that are the most important part of our study.

Local density gradients drive the stochastic motion of the cells[56]. Thus, one has,

$$\frac{\partial C(x, y, t)}{\partial t} = D\nabla^2 C(x, y, t), \tag{3}$$

where D is the diffusion coefficient. Equation (3) is applicable to the various kinds of cells, for which[16,57] $D \approx 10^{-10}$ cm^2/s. Population growth of biological groups depends on the species ability for proliferation and the environmental limitations. One important environmental limit is contact inhibition of cell division[58], i.e., if after the energy rises to u_p, the cells will duplicate if there is space; otherwise, they will stay quiescent until they find space for duplication[59]. Thus, proliferation at each site depends on the number of cells that can duplicate, and the effect of competition for space between all types of cells. The evolution of the CSCs that qualifies for the duplication metabolic threshold u_p, is expressed by a diffusion-reaction equation,

$$\begin{aligned}\frac{\partial C_{CSC}(x, y, t)}{\partial t} &= D\nabla^2 C_{CSC}(x, y, t) \\ &\quad + R_m p_s C_{CSC}(x, y, t)[1 - C_t(x, y, t)],\end{aligned} \tag{4}$$

where R_m is the rate of passing the S, G_2 and M phases in the cell cycle, which is fixed as a cell that has enough internal energy (has passed the aforementioned eG_1, G_1 and eS phases) will duplicate in 5 hours[46], if there were no other cells. The last term on the right side of Eq. (5) that includes the term $[1 - C_t(x, y, t)]$ captures the effect of contact inhibition of proliferation in which $C_t(x, y, t)$ is the total density of all cells at (x, y, t). The entire cell cycle takes 20 h. The evolution of the jth generation of the CCs is governed by

$$\begin{aligned}\frac{\partial C_{CC}(x, y, t; j)}{\partial t} &= D\nabla^2 C_{CC}(x, y, t; j) \\ &\quad + \delta_{1j} R_m [1 - p_s][1 - C_t(x, y, t)] \\ &\quad + (1 - \delta_{1j}) R_m C_{CC}(x, y, t; j - 1)[1 - C_t(x, y, t)] \\ &\quad - (1 - \delta_{jg}) R_m C_{CC}(x, y, t; j)[1 - C_t(x, y, t)] \\ &\quad - \delta_{jg} R_a C_{CC}(x, y, t; j),\end{aligned} \tag{5}$$

where δ_{ij} denotes the Kronecker delta, i.e., $\delta_{ij} = 1$ for $i = j$ and 0 otherwise, with $1 \leq i, j \leq g$. The first term on the right side of Eq. (5) represents diffusion of the cells due to the local concentration gradient;[16,56] the second is the creation of the first generation of the CCS due to asymmetric duplication of the CSCs[10], while the third term represents the creation of the jth generation (for $j \neq 1$) of the CCs from duplication of the prior generation. The concentration of the CCs decreases due to duplication and creation of the next generation, which the 4th terms accounts for, while the last term takes into account the death of the final (gth) generation of the CCs. R_a is the rate of apoptosis - the process of programmed cell death - and is fixed as the gth generation has a halflife equal to 1 day. Finally, the evolution of the oxygen density in the presence of the cells is governed by

$$\frac{\partial n(x, y, t)}{\partial t} = \beta \nabla^2 n(x, y, t) - \alpha[C_{\mathrm{CSC}}(x, y, t) + \sum_{j=1}^{g} C_{\mathrm{CC}}(x, y, t; j)], \tag{6}$$

with α being proportional to oxygen consumption rate by the cells, which is the same for both the CCs and cancerous stem cells. We varied the rates of oxygen consumption for every kind of cells, but the essential results remained the same; see the SI. α was fixed by setting the reported value for oxygen consumption[16,60] to be 6.65×10^{-17} mol cell^{-1} s^{-1}. β is the diffusion coefficient of oxygen in the medium, which we fixed it based on the calculations at room temperature, 10^{-5} cm^2/s. We present in the SI the results for other values of β. For distances more than 1 cm from the medium's center the oxygen density is constant (see the SI for the results for larger and smaller distances, as well as other ways of supplying the oxygen), and is equal to 0.15 mol/ml[16]. For simplicity, in all the calculations we normalize n to 1. From outside of the aforementioned circle, oxygen penetrates into the central area. Given the assumptions, the cells are active elastic species, consuming oxygen and proliferating.

As we show in the SI, other boundary conditions do not change the essential results. In addition, (i) we also varied both the proliferation activity and oxygen consumption rate for various kinds of cells, but the results remained qualitatively the same. (ii) The CSCs and CCs are assumed to have equal oxygen consumption rates, but when we changed them for every kind of cell, the results were qualitatively the same. (iii) The CSCs and CCs are assumed to have the same internal energy threshold u_p for duplication, and equal rates of crossing the S, G_2 and M phases in the cell cycle. But changing the proliferation activity of the cells did not change our main results. Let us also emphasize that our model is not the same as the classical models of diffusion-limited aggregation[61], as such model did not deal with the effect of reaction and consumption.

References

1. Reya, T., Morrison, S. J., Clarke, M. F. & Weissman, I. L. Stem cells, cancer, and cancer stem cells. *nature* **414**, 105–111 (2001).
2. Beck, B. & Blanpain, C. Unravelling cancer stem cell potential. *Nature Reviews Cancer* **13**, 727–738 (2013).
3. Quintana, E. *et al*. Efficient tumour formation by single human melanoma cells. *Nature* **456**, 593–598 (2008).
4. Medema, J. P. Cancer stem cells: the challenges ahead. *Nature cell biology* **15**, 338–344 (2013).
5. Li, S. & Li, Q. Cancer stem cells and tumor metastasis. *International journal of oncology* **44**, 1806–1812 (2014).
6. Liu, H. *et al*. Cancer stem cells from human breast tumors are involved in spontaneous metastases in orthotopic mouse models. *Proceedings of the National Academy of Sciences* **107**, 18115–18120 (2010).
7. Lin, X. *et al*. Notch4+ cancer stem-like cells promote the metastatic and invasive ability of melanoma. *Cancer science* **107**, 1079–1091 (2016).
8. Choi, D. *et al*. Cancer stem cell markers cd133 and cd24 correlate with invasiveness and differentiation in colorectal adenocarcinoma. *World journal of gastroenterology: WJG* **15**, 2258 (2009).
9. Enderling, H., Hlatky, L. & Hahnfeldt, P. Cancer stem cells: a minor cancer subpopulation that redefines global cancer features. *Breast* **11**, 200 (2013).
10. Sottoriva, A. *et al*. Cancer stem cell tumor model reveals invasive morphology and increased phenotypical heterogeneity. *Cancer research* **70**, 46–56 (2010).
11. Castellón, E. A. *et al*. Molecular signature of cancer stem cells isolated from prostate carcinoma and expression of stem markers in different gleason grades and metastasis. *Biological research* **45**, 297–305 (2012).
12. Vaupel, P., Kallinowski, F. & Okunieff, P. Blood flow, oxygen and nutrient supply, and metabolic microenvironment of human tumors: a review. *Cancer research* **49**, 6449–6465 (1989).
13. Höckel, M. *et al*. Association between tumor hypoxia and malignant progression in advanced cancer of the uterine cervix. *Cancer research* **56**, 4509–4515 (1996).
14. Cristini, V. *et al*. Morphologic instability and cancer invasion. *Clinical Cancer Research* **11**, 6772–6779 (2005).
15. Anderson, A. R., Weaver, A. M., Cummings, P. T. & Quaranta, V. Tumor morphology and phenotypic evolution driven by selective pressure from the microenvironment. *Cell* **127**, 905–915 (2006).
16. Anderson, A. R. A hybrid mathematical model of solid tumour invasion: the importance of cell adhesion. *Mathematical Medicine and Biology* **22**, 163–186 (2005).
17. Brú, A. *et al*. Super-rough dynamics on tumor growth. *Physical Review Letters* **81**, 4008 (1998).
18. Caldwell, C. B. *et al*. Characterisation of mammographic parenchymal pattern by fractal dimension. *Physics in medicine and biology* **35**, 235 (1990).
19. Lee, T. K. & Claridge, E. Predictive power of irregular border shapes for malignant melanomas. *Skin Research and Technology* **11**, 1–8 (2005).
20. Baish, J. W. & Jain, R. K. Fractals and cancer. *Cancer research* **60**, 3683–3688 (2000).
21. Tracqui, P. Biophysical models of tumour growth. *Reports on Progress in Physics* **72**, 056701 (2009).
22. Vasiev, B. N. Classification of patterns in excitable systems with lateral inhibition. *Physics Letters A* **323**, 194–203 (2004).
23. Vasiev, B., Hogeweg, P. & Panfilov, A. Simulation of dictyostelium discoideum aggregation via reaction-diffusion model. *Physical Review Letters* **73**, 3173 (1994).
24. Vasieva, O., Vasiev, B., Karpov, V. & Zaikin, A. A model of dictyostelium discoideum aggregation. *Journal of theoretical biology* **171**, 361–367 (1994).
25. Amar, M. B., Chatelain, C. & Ciarletta, P. Contour instabilities in early tumor growth models. *Physical review letters* **106**, 148101 (2011).
26. Tambasco, M., Eliasziw, M. & Magliocco, A. M. Morphologic complexity of epithelial architecture for predicting invasive breast cancer survival. *Journal of translational medicine* **8**, 140 (2010).

27. Etehad Tavakol, M., Lucas, C., Sadri, S. & Ng, E. Analysis of breast thermography using fractal dimension to establish possible difference between malignant and benign patterns. *Journal of Healthcare Engineering* **1**, 27–43 (2010).
28. Zook, J. M. & Iftekharuddin, K. M. Statistical analysis of fractal-based brain tumor detection algorithms. *Magnetic Resonance Imaging* **23**, 671–678 (2005).
29. Pérez, J. L. *et al*. Relationship between tumor grade and geometrical complexity in prostate cancer. *bioRxiv* 015016 (2015).
30. Smitha, K., Gupta, A. & Jayasree, R. Fractal analysis: fractal dimension and lacunarity from mr images for differentiating the grades of glioma. *Physics in medicine and biology* **60**, 6937 (2015).
31. Pribic, J. *et al*. Fractal dimension and lacunarity of tumor microscopic images as prognostic indicators of clinical outcome in early breast cancer. *Biomarkers* **9**, 1279–1277 (2015).
32. Buczko, O. & Mikołajczak, P. Shape analysis of mr brain images based on the fractal dimension. *Annales Universitatis Mariae Curie-Sklodowska, sectio AI–Informatica* **3**, 153–158 (2015).
33. Srivastava, A., Laidler, P., Hughes, L. E., Woodcock, J. & Shedden, E. J. Neovascularization in human cutaneous melanoma: a quantitative morphological and doppler ultrasound study. *European Journal of Cancer and Clinical Oncology* **22**, 1205–1209 (1986).
34. Brú, A., Albertos, S., Subiza, J. L., Garca-Asenjo, J. L. & Brú, I. The universal dynamics of tumor growth. *Biophysical journal* **85**, 2948–2961 (2003).
35. Hermann, P. C. *et al*. Distinct populations of cancer stem cells determine tumor growth and metastatic activity in human pancreatic cancer. *Cell stem cell* **1**, 313–323 (2007).
36. Girouard, S. D. & Murphy, G. F. Melanoma stem cells: not rare, but well done. *Laboratory investigation* **91**, 647–664 (2011).
37. Tang, X. *et al*. Cystine deprivation triggers programmed necrosis in vhl-deficient renal cell carcinomas. *Cancer research* **76**, 1892–1903 (2016).
38. Li, H. *et al*. Dt-13, a saponin monomer of dwarf lilyturf tuber, induces autophagy and potentiates anti-cancer effect of nutrient deprivation. *European Journal of Pharmacology* (2016).
39. Hilfinger, A. & Paulsson, J. Separating intrinsic from extrinsic fluctuations in dynamic biological systems. *Proceedings of the National Academy of Sciences* **108**, 12167–12172 (2011).
40. Berg, O. G., Paulsson, J. & Ehrenberg, M. Fluctuations and quality of control in biological cells: zero-order ultrasensitivity reinvestigated. *Biophysical journal* **79**, 1228–1236 (2000).
41. Trepat, X. *et al*. Physical forces during collective cell migration. *Nature physics* **5**, 426–430 (2009).
42. Wang, Y. *et al*. Fiber-laser-based photoacoustic microscopy and melanoma cell detection. *Journal of biomedical optics* **16**, 011014–011014 (2011).
43. Buchakjian, M. R. & Kornbluth, S. The engine driving the ship: metabolic steering of cell proliferation and death. *Nature reviews Molecular cell biology* **11**, 715–727 (2010).
44. Jones, R. G. & Thompson, C. B. Tumor suppressors and cell metabolism: a recipe for cancer growth. *Genes & development* **23**, 537–548 (2009).
45. Scalerandi, M. & Sansone, B. C. Inhibition of vascularization in tumor growth. *Physical review letters* **89**, 218101 (2002).
46. Haass, N. K. *et al*. Real-time cell cycle imaging during melanoma growth, invasion, and drug response. *Pigment cell & melanoma research* **27**, 764–776 (2014).
47. Meacham, C. E. & Morrison, S. J. Tumour heterogeneity and cancer cell plasticity. *Nature* **501**, 328–337 (2013).
48. Shahriyari, L. & Komarova, N. L. Symmetric vs. asymmetric stem cell divisions: an adaptation against cancer? *PLoS One* **8**, e76195 (2013).
49. Dhawan, A., Kohandel, M., Hill, R. & Sivaloganathan, S. Tumour control probability in cancer stem cells hypothesis. *PloS one* **9**, e96093 (2014).
50. Tomasetti, C. & Levy, D. Role of symmetric and asymmetric division of stem cells in developing drug resistance. *Proceedings of the National Academy of Sciences* **107**, 16766–16771 (2010).
51. Cao, Y., Naveed, H., Liang, C. & Liang, J. Modeling spatial population dynamics of stem cell lineage in wound healing and cancerogenesis. In *Engineering in Medicine and Biology Society (EMBC), 2013 35th Annual International Conference of the IEEE*, 5550–5553 (IEEE, 2013).
52. Yoo, M.-H. & Hatfield, D. L. The cancer stem cell theory: is it correct? *Molecules and cells* **26**, 514 (2008).
53. Gedye, C. *et al*. Cancer stem cells are underestimated by standard experimental methods in clear cell renal cell carcinoma. *Scientific reports* **6**, 25220 (2016).
54. Nowell, P. C. The clonal evolution of tumor cell populations. *Science* **194**, 23–28 (1976).
55. Hayflick, L. & Moorhead, P. S. The serial cultivation of human diploid cell strains. *Experimental cell research* **25**, 585–621 (1961).
56. Ambrosi, D. & Preziosi, L. On the closure of mass balance models for tumor growth. *Mathematical Models and Methods in Applied Sciences* **12**, 737–754 (2002).
57. Bray, D. *Cell movements: from molecules to motility* (Garland Science, 2001).
58. Martz, E. & Steinberg, M. S. The role of cell-cell contact in "contact" inhibition of cell division: A review and new evidence. *Journal of cellular physiology* **79**, 189–210 (1972).
59. Montel, F. *et al*. Stress clamp experiments on multicellular tumor spheroids. *Physical review letters* **107**, 188102 (2011).
60. Casciari, J. J., Sotirchos, S. V. & Sutherland, R. M. Variations in tumor cell growth rates and metabolism with oxygen concentration, glucose concentration, and extracellular ph. *Journal of cellular physiology* **151**, 386–394 (1992).
61. Gerlee, P. & Anderson, A. R. Diffusion-limited tumour growth: simulations and analysis. *Mathematical biosciences and engineering: MBE* **7**, 385 (2010).

Acknowledgements

A.A.S. would like to acknowledge support from the Alexander von Humboldt Foundation, and partial financial support from the research council of the University of Tehran. We also acknowledge the High Performance Computing center of the University of Tehran in its Department of Physics, where most of computations were carried out. We thank an anonymous referee for constructive criticisms that guided us to revise and improve the manuscript.

Author Contributions

A.A.S. proposed the project and computations. Y.A. did the simulations. Y.A., A.A.S. and M.S. analyzed the data and wrote the paper.

Additional Information

Supplementary information accompanies this paper at https://doi.org/10.1038/s41598-018-24418-8.

Competing Interests: The authors declare no competing interests.

Publisher's note: Springer Nature remains neutral with regard to jurisdictional claims in published maps and institutional affiliations.